1 **Assessing snow extent data sets over North America to inform and improve trace gas**

2 **retrievals from solar backscatter**

3 Matthew J. Cooper[1], Randall V. Martin[1,2], Alexei I. Lyapustin[3], and Chris A. McLinden[4]

4 1. Department of Physics and Atmospheric Science, Dalhousie University, Halifax, Nova Scotia,

5 Canada.

6 2. Harvard-Smithsonian Center for Astrophysics, Cambridge, Massachusetts, USA

7 3. NASA Goddard Space Flight Center, Greenbelt, MD, USA

8 4. Air Quality Research Division, Environment and Climate Change Canada, Toronto, Ontario,

9 Canada

10 **Abstract**

11 Accurate representation of surface reflectivity is essential to tropospheric trace gas retrievals

12 from solar backscatter observations. Surface snow cover presents a significant challenge due to

13 its variability and thus snow-covered scenes are often omitted from retrieval data sets; however,

14 the high reflectance of snow is advantageous for trace gas retrievals. We first examine the

15 implications of surface snow on retrievals from the upcoming TEMPO geostationary instrument

16 for North America. We use a radiative transfer model to examine how an increase in surface

17 reflectivity due to snow cover changes the sensitivity of satellite retrievals to NO_2 in the lower

18 troposphere. We find that a substantial fraction (>50%) of the TEMPO field of regard can be

19 snow covered in January, and that the average sensitivity to the tropospheric NO_2 column

20 substantially increases (doubles) when the surface is snow covered.

21 We then evaluate seven existing satellite-derived or reanalysis snow extent products against

22 ground station observations over North America to assess their capability of informing surface

23 conditions for TEMPO retrievals. The Interactive Multisensor Snow and Ice Mapping System

24 (IMS) had the best agreement with ground observations (accuracy=93%, precision=87%,

25 recall=83%). Multiangle Implementation of Atmospheric Correction (MAIAC) retrievals of

26 MODIS observed radiances had high precision (90% for Aqua and Terra), but underestimated

27 the presence of snow (recall=74% for Aqua, 75% for Terra). MAIAC generally outperforms the

28 standard MODIS products (precision=51%, recall=43% for Aqua; precision=69%, recall=45%

29 for Terra). The Near-real-time Ice and Snow Extent (NISE) product had good precision (83%)

30 but missed a significant number of snow covered pixels (recall=45%). The Canadian

31 Meteorological Centre (CMC) Daily Snow Depth Analysis Data set had strong performance

32 metrics (accuracy=91%, precision=79%, recall=82%). We use the F score, which balances

33 precision and recall, to determine overall product performance (F = 85%, 82(82)%, 81%, 58%,

34 46(54)% for IMS, MAIAC Aqua(Terra), CMC, NISE, MODIS Aqua(Terra) respectively) for

35 providing snow cover information for TEMPO retrievals from solar backscatter observations.

36 We find that using IMS to identify snow cover and enable inclusion of snow-covered scenes

37 across North America in January can increase both the number of observations by a factor of 2.1

38 and the average sensitivity to the tropospheric NO_2 column by a factor of 2.7.

39

1. Introduction

41   Satellite observations of solar backscatter are widely used as a source of information on

42 atmospheric trace gases (Richter and Wagner, 2011). These observations have provided valuable

43 information on vertical column densities of O_3, NO_2, SO_2, CO, HCHO, CH_4 and other important

44 trace gases in the troposphere (Fishman et al., 2008). Satellite observations of trace gases have

45 been used to assess air quality (Duncan et al., 2014; Martin, 2008) and to gain insight into

46 atmospheric processes including emissions (Streets et al., 2013), lifetimes (Beirle et al., 2011;

47 Fioletov et al., 2015; de Foy et al., 2015; Valin et al., 2013), and deposition (Geddes and Martin,

48 2017; Nowlan et al., 2014). The utility of these observations is dependent on their quality, and

49 thus ensuring retrieval accuracy is essential.

50   Previous studies have found that retrieved NO_2 vertical column densities are highly

51 sensitive to errors in assumed surface reflectance (Boersma et al., 2004; Lamsal et al., 2017;

52 Martin et al., 2002). Much of this error sensitivity results from observation sensitivity to trace

53 gases in the lower troposphere. The observation sensitivity is accounted for in the air mass factor

54 (AMF) conversion of observed line-of-sight "slant columns" to vertical column densities.

55 Uncertainties in surface reflectance are a significant contributor to AMF uncertainty.

56   Existing reflectivity climatologies (e.g. Kleipool et al., 2008; Koelemeijer et al., 2003;

57 Liang et al., 2002; Herman and Celarier, 1997) do not represent snow cover well, since the

58   statistical methods to exclude reflective clouds from the climatologies also exclude variable

59   snow cover; Correspondingly, surface snow may be mistaken for cloud, leading to errors in

60   cloud fraction and pressure estimates used in trace gas retrievals (Lin et al., 2015; O'Byrne et al.,

61   2010; Vasilkov et al., 2017). Therefore, snow cover is particularly challenging to retrievals.

62   Misrepresenting surface snow cover can lead to large errors (20-50%) in retrieved NO_2 columns

63   over broad regions with seasonal snow cover (O'Byrne et al., 2010). For this reason,

64   observations over snow are often omitted to avoid potential errors. This limits the ability of

65   satellite retrieved data sets to offer adequate temporal and spatial sampling in winter months.

66   Additionally, over highly reflective surfaces such as snow observation sensitivity to the lower

67   troposphere is larger and has less dependence on *a priori* NO_2 profiles (Lorente et al., 2017;

68   O'Byrne et al., 2010); Thus, omitting snow-covered scenes means omitting the observations with

69   the greatest sensitivity to the lower troposphere. This could be remedied by using a product that

70   would allow for snow cover identification to be done with confidence.

71   Several data products provide information on snow extent using surface station

72   observations, satellite observed radiances, or visible imagery. Previous evaluations have found it

73   difficult to determine which of these products is definitively the best, partly due to differences in

74   resolution. Most products are more consistent during the winter months when persistent, deep

75   snow is present (Frei et al., 2012; Frei and Lee, 2010). However, disagreements are common

76   during accumulation and melting seasons, over mountains, and under forest canopies. These

77   evaluations have largely focused on local or regional snow cover, or included only cloud-free

78   observations.

79   The upcoming geostationary Tropospheric Emissions: Monitoring of Pollution (TEMPO)

80   satellite instrument will provide hourly observations of air quality relevant trace gases over

81   North America at an unprecedented spatial and temporal resolution (Zoogman et al., 2017). As is

82   the case for all nadir satellite retrievals, the quality of these observations will depend on the

83   accuracy of the surface reflectance used in the retrieval. As a significant portion of the observed

84   domain experiences snow cover, an accurate representation of snow cover is needed. Current

85   plans to deal with snow cover for TEMPO are to rely on external observations.

86   In this work, we examine the importance of accurate snow identification by using a

87   radiative transport model to evaluate how the vertical sensitivity of a satellite retrieval is

88   impacted by surface reflectance. We then assess seven snow extent products that are expected to

89   continue to be operational during the TEMPO mission using in situ observations across North

90   America with the intent of determining which product is best suited for providing snow cover

91   information for TEMPO and other future satellite retrievals. Finally, we combine radiative

92   transfer model results with a snow extent product to show how including snow-covered scenes

93   improves both the quantity and quality of information in a retrieval data set.

94

95   **2. Data and Algorithms**

96   **2.1. Gridded Snow Products**

97   **2.1.1. IMS**

98   One of the most widely used sources of snow extent data is the Interactive Multisensor

99   Snow and Ice Mapping System (IMS). IMS provides daily, near-real-time maps of snow and sea

100 ice cover in the Northern Hemisphere at 4km resolution (Helfrich et al., 2007). The maps are

101 produced by a trained analyst using visible imagery from a collection of geostationary (e.g.

102 GOES, MeteoSat) and polar orbiting (e.g. AVHRR, MODIS, SAR) satellite instruments, with

103 additional information from microwave sensors (e.g. DMSP, AMSR, AMSU), surface

104 observations (e.g. SNOTEL), and models (e.g. SNODAS) (Helfrich et al., 2007). By using

105 multiple sources of information with different spatial resolution and temporal sampling, IMS can

106 minimize interference from clouds.

107   **2.1.2. MODIS**

108   A second commonly used snow and ice product is derived from MODIS satellite

109 observations from the Terra and Aqua satellites (Hall and Riggs, 2007). Terra and Aqua have

110 sun-synchronous, near polar orbits with overpass times of 1030 and 1330 hr respectively. Snow

111 cover is calculated using a Normalized Difference Snow Index (NDSI), which examines the

112 difference between observed radiation at visible wavelengths (where snow is highly reflective)

113 and short IR wavelengths (where there is little reflection from snow). Observations are made at

114 500 m spatial resolution and aggregated to produce daily snow cover fractions on a 0.05°

115 resolution grid. Past evaluations of the standard MODIS snow product show good agreement in

cloud-free conditions but often snow is misidentified as cloud (Hall and Riggs, 2007; Yang et al., 2015).

The Multiangle Implementation of Atmospheric Correction (MAIAC) algorithm is another algorithm processing MODIS observations. MAIAC retrievals uses radiances observed by the MODIS Aqua and Terra satellites to provide atmospheric and surface products including snow detection on a 1 km grid (Lyapustin et al., 2011a, 2011b, 2012). While the NDSI used by the standard MODIS product is also used by MAIAC as one of the criteria, the overall snow and cloud detection in MAIAC are different from the standard MODIS algorithm (Lyapustin et al., 2008).

2.1.3. NISE

The Near-real-time Ice and Snow Extent (NISE) provides daily updated snow cover extent information on a 25x25 km grid (Nolin et al., 2005). NISE uses microwave measurements from the Special Sensor Microwave Imager/Sounder (SSM/I) on a sun-synchronous, quasi-polar orbit to observe how microwave radiation emitted by soil is scattered by snow. Products based on microwave measurements such as NISE are known to miss wet and thin snow, as wet snow emits microwave radiation similar to soil, and thin snow does not provide sufficient scattering.

2.1.4. CMC

The Canadian Meteorological Centre (CMC) Daily Snow Depth Analysis Data is a statistical interpolation of snow depth measurements from 8,000 surface sites across Canada and U.S. interpolated using a snow pack model (Brasnett, 1999). Unlike the aforementioned satellite products that provide snow extent, CMC provides snow depths. Daily snow maps are produced at 25 km resolution. As it a reanalysis product, there is a time delay in availability. The CMC snow depths show good agreement with independent observations over midlatitudes and is considered an improvement over previous snow depth climatologies (Brown et al., 2003).

2.2 Surface observations

These snow identification products are evaluated against surface station observations from the Global Historical Climatology Network-Daily (GHCN-D) database, an amalgamation of daily climate records from over 80,000 surface stations worldwide (Menne et al., 2012a).

144 Most observations over Canada and the United States are collected by government organizations

145 (Environment and Climate Change Canada and NOAA National Climatic Data Center,

146 respectively) with additional measurements from smaller observation networks. While the focus

147 of the database is collecting temperature and precipitation measurements, many stations (1,279 in

148 Canada, 13,932 in United States in 2015 used here) also offer snow depth measurements.

149   A subset of the surface stations included in GHCN-D may also be used in the CMC

150 reanalysis. It is difficult to definitively know which stations are used, as CMC does not routinely

151 archive this information. However, we estimate that only 5% of the GHCN-D stations used here

152 are located within 0.1° of a possible CMC station, and thus GHCN-D has sufficient independent

153 information sources to evaluate the CMC product.

154   **2.3 Radiative transfer calculations**

155   The sensitivity of satellite observations of NO_2 to its vertical distribution is calculated

156 here using the LIDORT radiative transfer model (Spurr, 2002). The model is used to calculate

157 scattering weights, which quantify the sensitivity of backscattered solar radiation to NO_2 at

158 different altitudes (Martin et al., 2002; Palmer et al., 2001). The observation sensitivity to lower

159 tropospheric NO_2 is represented by the air mass factor. Air mass factors for OMI satellite

160 observations in January 2013 are calculated as a useful analog for future TEMPO observations as

161 both instruments are spectrometers observing reflected sunlight at UV to visible wavelengths.

162 AMFs are calculated at 440 nm, at the centre of the NO_2 retrieval window for OMI and TEMPO

163 where NO_2 has strong absorption features. Vertical NO_2 profiles, and other trace gas and aerosol

164 profiles needed for the AMF calculation shown here, are obtained from a simulation of the

165 GEOS-Chem chemical transport model version 11-01 (www.geos-chem.org).

166   Figure 1 shows maps of snow-free and snow-covered reflectances used here. Snow-free

167 surface reflectance at 470 nm is provided by Nadir BRDF-Adjusted reflectances from the

168 MODIS CMG Gap-Filled Snow-Free Products (Sun et al., 2017). Reflectivities at 354 nm for

169 snow-covered scenes are derived from OMI observations as described by O'Byrne et al. (2010).

170 While this wavelength is different than the 440 nm wavelength used to calculate AMFs, snow

171 reflectivity has weak spectral dependence in UV-Visible wavelengths (Feister and Grewe, 1995;

172 O'Byrne et al., 2010). Snow can increase surface reflectance by over a factor of 10 in central

173 North America where short vegetation is readily covered by snow.

3. Methods

Here we test daily snow cover products for 2015. Snow products are regridded from their native resolutions to a common 4 km grid (similar to the spatial resolution of TEMPO). A grid box is considered to be snow covered if any observations within that box are snow covered. MAIAC, NISE, and IMS give only a yes/no flag for presence of snow. MODIS products provide a pixel snow fraction, and we consider any pixels with nonzero snow fractions as snow covered. Any CMC grid box with nonzero snow depth is considered snow covered.

GHCN-D surface measurements are used as the ground "truth" for evaluating the satellite and reanalysis snow data products tested here. If measurements from multiple surface data networks exist in the same grid box, the most reliable source is used per the priority order given by GHCN-D (Menne et al., 2012b). If observations from multiple surface stations within the most reliable network within a grid box disagree on the presence of snow on a given day, that day is excluded from the evaluation.

We assess the snow data sets using metrics that are commonly used for evaluating binary data sets (Rittger et al., 2013). These metrics are based on the possible outcomes for identifying snow: true positive (TP), true negative (TN), false positive (FP), and false negative (FN). Accuracy measures the likelihood that a grid box, with snow or without, is correctly classified:

$$Accuracy = \frac{TP + TN}{TP + TN + FP + FN} \tag{1}$$

Precision is the probability that a region identified as snow-covered has snow:

$$Precision = \frac{TP}{TP + FP} \tag{2}$$

Recall is the likelihood that snow cover is detected when present:

$$Recall = \frac{TP}{TP + FN} \tag{3}$$

The *F* score balances recall (which accounts for false negatives) and precision (which accounts for false positives) to measure correct classification of snow without the influence of frequent snow-free periods, and therefore is the metric which is most relevant for TEMPO:

$$F = 2 * \frac{precision * recall}{precision + recall} \qquad (4)$$

4. Results

We first examine the effect of surface reflectivity on retrieval sensitivity by using the LIDORT radiative transfer model to calculate NO_2 air mass factors for both snow-free and snow-covered scenarios over North America. We calculate air mass factors over North America in January 2013. We assume cloud-free conditions in all AMF calculations, as the impact of surface reflectance on retrieved cloud fractions is beyond the scope of this paper.

Figure 2 shows the sensitivity of backscattered radiation (scattering weights) over snow-covered and snow-free surfaces for two locations; a midlatitude location (US Midwest, 42°N, 99°W) with a solar zenith angle of 60° and at a high latitude location (Northern Canada, 58°N, 76°W) with a solar zenith angle of 79°. The snow-covered scattering weights are greater than the snow-free scattering weights throughout the troposphere, by factors of 2.0 (2.7) below 5 km, 2.7 (3.7) below 2 km, and 2.6 (5.3) below 1 km at the mid (high) latitude location. This shows that satellite observed backscattered radiation is up to five times as sensitive to NO_2 in the boundary layer in the presence of snow, due to the increased absorption by NO_2 in the lower troposphere when the surface reflects more sunlight.

Figure 3 shows the distribution of AMF values over North America with and without reflectance from snow. The snow-free AMF distribution is unimodal with a median of 1.2. Allowing for the presence of snow introduces a second mode with a median of 3.2. Mean AMFs increase by a factor 2.0 in the presence of snow, indicating an overall doubling in the sensitivity to tropospheric NO_2 over snow covered surfaces across North America. The impact is larger over polluted regions, as mean AMFs increase by a factor of 2.2 in regions where NO_2 columns exceed $1x10^{15}$ molec/cm^2. Maps of AMF with and without snow cover for January 2013 show that AMF values increase over 69% of the land surface within the TEMPO domain.

We next examine the snow datasets to identify the one most suited for the TEMPO retrieval algorithm. Figure 4 shows the spatial distribution of false positives and false negatives in the data sets. In all data sets, both false positives and negatives are most frequent over mountainous regions, particularly in the Rocky Mountain region, consistent with previous validation studies (Chen et al., 2012, 2014; Frei et al., 2012; Frei and Lee, 2010). These errors

224   are often attributed to differences in representativeness, as snow cover in mountain regions is

225   often spatially inhomogeneous, and thus *in situ* measurements may not be representative of the

226   pixel. A slight increase in the number of false positives in IMS over mid-western and prairie

227   regions may result from crop regions with high snow-free albedos being mistaken for snow in

228   visible imagery (Chen et al., 2012; Yang et al., 2015). NISE, MODIS Aqua, and MODIS Terra

229   have more false negatives overall, especially in the Great Lakes and New England regions. False

230   positives are less frequent than false negatives in all data sets. IMS and CMC have the lowest

231   frequency of false negatives. NISE and MAIAC have the lowest frequency of false positives.

232   Figure 5 shows the metrics used to evaluate data set performance. Table 1 summarizes

233   these results. All data sets have high accuracy numbers, owing largely to a high number of true

234   negatives during the summer months. MODIS Aqua and Terra have low recall and *F* scores.

235   When only observations with MODIS cloud fractions less than 20% are used, MODIS has better

236   agreement with the ground stations (*F* statistic increases from 0.38 to 0.49 at native resolution

237   for Aqua, 0.43 to 0.63 for Terra), however this reduces the number of usable MODIS

238   observations by up to 60%. NISE has high precision but low recall, indicating that while areas

239   classified as snow-covered by NISE are likely correct, many snow-covered regions are missing

240   in the data set. This is consistent with evaluations by McLinden et al. (2014) and O'Byrne et al.

241   (2010). Although CMC, IMS, and MAIAC products show an increase in frequency of false

242   negatives over the Rocky Mountains, they retain a high precision in this region due to frequent

243   snow cover. While MAIAC Aqua/Terra have high accuracy and precision, lower recall values

244   indicate that they are conservative in identifying the presence of snow. This is possibly a

245   consequence of the method used for identifying cloud, which may incorrectly classify fresh

246   snowfall as cloud (Lyapustin et al., 2008). Data sets were also evaluated by season with similar

247   results (Appendix Table A1). All data sets have weaker performance metrics during the spring

248   melt season, which has been observed in past evaluations (Frei et al., 2012). IMS has the highest

249   *F* score in winter and autumn but is slightly outperformed by MAIAC in spring. Data sets were

250   also evaluated at their native resolutions and at a common 25 km resolution (Appendix Tables

251   A2-3). Results are similar at each resolution with two exceptions: MODIS Aqua and Terra

252   products perform better when regridded from their native 0.05° resolution to a 4 km resolution as

253   it reduces the number of grid boxes missing observations due to cloud, and MAIAC Aqua and

254 Terra perform better at their native resolution than at either 4 km or 25 km as degrading the
255 spatial resolution results in a loss of information.

256   For all data sets, recall is generally low in two regions: along the Pacific coastline where
257 snow depths are relatively thin, and in the south when snow is rare and generally short lived.
258 Thin snow is likely to be less homogenous across a pixel and more likely to be obscured by
259 forest canopies or tall grasses, and thus is difficult to observe from satellite imagery. Short lived
260 snow in the south is likely to be missed by satellite observations, especially since clouds are
261 often present. However, as IMS uses multiple observations at multiple times of day in addition to
262 incorporating ground station data, it is more likely to find snow in these cases than other satellite
263 products (Hall et al., 2010). Overall, IMS has best agreement with *in situ* observations, with the
264 highest accuracy, recall, and *F* statistic and relatively high precision.

265   While CMC also has strong performance metrics, it is important to consider the
266 information source used to describe snow extent in each product. Products based on satellite
267 observations are advantageous when assessing how surface reflectivity affects backscattered
268 radiation observed from space. For example, thin snow, or snow obscured by tree canopies, may
269 not affect the observed brightness from space, but would be considered snow-covered by a
270 product based on surface observations (e.g. CMC). Also, the reflectivity of a snow-covered
271 surface decreases over time as the snow ages (Warren and Wiscombe, 1980); This effect would
272 not be captured by snow depth measurements. And while snow depth has been used as an
273 indicator of brightness (Arola et al., 2003), it can not account for snow aging or canopy effects.
274 IMS is based on visible satellite imagery and thus determines snow extent based on brightness
275 from space, which is more applicable to satellite retrievals. And while most satellite-based
276 products rely on observations made at a single overpass time and viewing geometry, IMS has the
277 advantage of incorporating observations from multiple satellites with differing measurement
278 times and geometries, including both geostationary and low Earth orbits. These reasons, in
279 addition to a strong agreement with in situ measurements and near-real-time updates, make IMS
280 best suited for informing TEMPO retrievals.

281   We next examine the effect on both spatial sampling and sensitivity to the lower
282 troposphere of a retrieval data set if observations with surface snow are included rather than
283 omitted. We use IMS to identify the presence of snow for OMI observations over North America

284 in January 2015. We then use LIDORT to calculate AMFs for these observations using the

285 corresponding snow-free (Sun et al., 2017) or snow-covered (O'Byrne et al., 2010) surface

286 reflectance, and examine the results of either including or omitting snow-covered scenes. Figure

287 6 shows that including snow-covered scenes results in a significant (factor of 2.1) increase in

288 observation frequency, particularly in the northern US and Canada. Additionally, including

289 snow-covered scenes increases the average AMF by a factor of 2.7 in regions with occasional

290 snow cover. The increase in AMF demonstrates that including snow-covered scenes increases

291 the quality of information about the tropospheric NO_2 column by increasing the observation

292 sensitivity to tropospheric NO_2.

293

294 5. Conclusion

295   An accurate representation of snow cover is essential to ensuring satellite retrieval

296 accuracy, including those from TEMPO. Radiative transfer model calculations indicate that NO_2

297 retrievals over reflective snow-covered surfaces are more than twice as sensitive to NO_2 in the

298 boundary layer than over snow-free surfaces. This makes snow an attractive surface over which

299 to observe tropospheric NO_2. However, the lack of confidence in snow identification has

300 previously led many retrieval procedures to omit observations over snow. We show that

301 increasing this confidence such that these observations could be included not only improves

302 spatial and temporal sampling, but also allows the inclusion of observations with higher quality

303 information on the lower troposphere.

304   We evaluated seven snow extent data sets to determine their usefulness for informing

305 satellite retrievals of trace gas from solar backscatter observations. All products were more likely

306 to misidentify snow over mountains or where snow cover is thin or short lived. IMS had the best

307 agreement with *in situ* observations (F=0.85), and as a satellite based, operational, daily updated

308 product, it is well suited for informing TEMPO satellite retrievals. The low recall value (0.45)

309 for NISE indicated that a significant number of snow covered pixels are missed. The standard

310 MODIS products showed medium precision and low recall owing to cloud contamination. The

311 MAIAC products had the highest precision (0.90 for both Aqua and Terra) of those tested, but is

312 conservative in ascribing the presence of snow (recall=0.74 for Aqua, 0.75 for Terra). CMC had

313 strong performance metrics (F=0.81), but as a reanalysis product based on ground observations it

314 may not appropriately represent how a surface snow reflectivity would affect TEMPO observed

315 radiances.

316   Future work should investigate snow reflectance products that could be used when snow

317 is detected. This could potentially include Bidirectional Reflectance Distribution Functions

318 (BRDF) that describe reflection at different viewing angles, as this effect has been shown to have

319 significant impact on retrieved NO_2 columns (Vasilkov et al., 2017). A retrieval algorithm that

320 combines daily snow detection from IMS with a climatology of snow reflectance has the

321 potential to greatly improve upon current methodologies.

322

323 6. Data Availability

324   IMS (National Ice Center, 2008), NISE (Brodzik and Stewart, 2016), MODIS Aqua (Hall

325 and Riggs, 2016a), MODIS Terra (Hall and Riggs, 2016b), and CMC (Brown and Brasnett,

326 2010) data are available from the NASA National Snow and Ice Data Center (http://nsidc.org).

327 MAIAC Collection 6 re-processing of MODIS data started in September 2017 and is expected to

328 be completed by the end of year. This study used MAIAC data currently available via ftp at

329 NASA Center for Climate Simulations (NCCS):

330 ftp://maiac@dataportal.nccs.nasa.gov/DataRelease/. GHCN-D data are available from the

331 NOAA National Climatic Data Center (Menne et al., 2012b; www.ncdn.noaa.gov). Code for

332 calculating scattering weights and air mass factors, and snow-covered surface reflectances used

333 here are available at http://fizz.phys.dal.ca/~atmos. Snow-free surface reflectances are available

334 at ftp://rsftp.eeos.umb.edu/data02/Gapfilled/. The GEOS-Chem chemical transport model used

335 here is available at www.geos-chem.org.

336 7. References

337 Arola, A., Kaurola, J., Koskinen, L., Tanskanen, A., Tikkanen, T., Taalas, P., Herman, J. R.,

338 Krotkov, N. and Fioletov, V.: A new approach to estimating the albedo for snow-covered

339 surfaces in the satellite UV method, J. Geophys. Res., 108(D17), 4531,

340 doi:10.1029/2003JD003492, 2003.

341 Beirle, S., Boersma, K. F., Platt, U., Lawrence, M. G. and Wagner, T.: Megacity emissions and

342 lifetimes of nitrogen oxides probed from space., Science, 333(6050), 1737–9,

343 doi:10.1126/science.1207824, 2011.

344 Boersma, K. F., Eskes, H. J. and Brinksma, E. J.: Error analysis for tropospheric NO2 retrieval

345 from space, J. Geophys. Res. Atmos., 109(D4), 2004.

346 Brasnett, B.: A Global Analysis of Snow Depth for Numerical Weather Prediction, J. Appl.

347 Meteorol., 38(6), 726–740, doi:10.1175/1520-0450(1999)038<0726:AGAOSD>2.0.CO;2, 1999.

348 Brodzik, M. J. and Stewart, J. S.: Near-Real-Time SSM/I-SSMIS EASE-Grid Daily Global Ice

349 Concentration and Snow Extent, Version 5, , doi:http://dx.doi.org/10.5067/3KB2JPLFPK3R,

350 2016.

351 Brown, R. D. and Brasnett, B.: Canadian Meteorological Centre (CMC) Daily Snow Depth

352 Analysis Data, Version 1, , doi:http://dx.doi.org/10.5067/W9FOYWH0EQZ3, 2010.

353 Brown, R. D., Brasnett, B. and Robinson, D.: Gridded North American monthly snow depth and

354 snow water equivalent for GCM evaluation, Atmosphere-Ocean, 41(1), 1–14,

355 doi:10.3137/ao.410101, 2003.

356 Chen, C., Lakhankar, T., Romanov, P., Helfrich, S., Powell, A. and Khanbilvardi, R.: Validation

357 of NOAA-Interactive Multisensor Snow and Ice Mapping System (IMS) by Comparison with

358 Ground-Based Measurements over Continental United States, Remote Sens., 4(12), 1134–1145,

359 doi:10.3390/rs4051134, 2012.

360 Chen, X., Jiang, L., Yang, J. and Pan, J.: Validation of ice mapping system snow cover over

361 southern China based on Landsat Enhanced Thematic Mapper Plus imagery, J. Appl. Remote

362 Sens., 8(1), 84680, doi:10.1117/1.JRS.8.084680, 2014.

363 Duncan, B. N., Prados, A. I., Lamsal, L. N., Liu, Y., Streets, D. G., Gupta, P., Hilsenrath, E.,

364 Kahn, R. A., Nielsen, J. E., Beyersdorf, A. J., Burton, S. P., Fiore, A. M., Fishman, J., Henze, D.

365 K., Hostetler, C. A., Krotkov, N. A., Lee, P., Lin, M., Pawson, S., Pfister, G., Pickering, K. E.,

366 Pierce, R. B., Yoshida, Y. and Ziemba, L. D.: Satellite data of atmospheric pollution for U.S. air

367 quality applications: Examples of applications, summary of data end-user resources, answers to

368 FAQs, and common mistakes to avoid, Atmos. Environ., 94, 647–662,

369 doi:10.1016/j.atmosenv.2014.05.061, 2014.

370 Feister, U. and Grewe, R.: Spectral albedo measurements in the UV and visible region over

371 different types of surfaces, Photochem. Photobiol., 62(4), 736–744, doi:10.1111/j.1751-

372 1097.1995.tb08723.x, 1995.

373 Fioletov, V. E., McLinden, C. A., Krotkov, N. and Li, C.: Lifetimes and emissions of SO2 from

374 point sources estimated from OMI, Geophys. Res. Lett., 42(6), 1969–1976,

375 doi:10.1002/2015GL063148, 2015.

376 Fishman, J., Al-Saadi, J. A., Creilson, J. K., Bowman, K. W., Burrows, J. P., Richter, A.,

377 Chance, K. V., Edwards, D. P., Martin, R. V., Morris, G. A., Pierce, R. B., Ziemke, J. R.,

378 Schaack, T. K., Thompson, A. M., Fishman, J., Al-Saadi, J. A., Creilson, J. K., Bowman, K. W.,

379 Burrows, J. P., Richter, A., Chance, K. V., Edwards, D. P., Martin, R. V., Morris, G. A., Pierce,

380 R. B., Ziemke, J. R., Schaack, T. K. and Thompson, A. M.: Remote Sensing of Tropospheric

381 Pollution from Space, Bull. Am. Meteorol. Soc., 89(6), 805–821,

382 doi:10.1175/2008BAMS2526.1, 2008.

383 de Foy, B., Lu, Z., Streets, D. G., Lamsal, L. N. and Duncan, B. N.: Estimates of power plant NO

384 x emissions and lifetimes from OMI NO 2 satellite retrievals, Atmos. Environ., 116, 1–11, 2015.

385 Frei, A. and Lee, S.: A comparison of optical-band based snow extent products during spring

386 over North America, Remote Sens. Environ., 114(9), 1940–1948, doi:10.1016/j.rse.2010.03.015,

387 2010.

388 Frei, A., Tedesco, M., Lee, S., Foster, J., Hall, D. K., Kelly, R. and Robinson, D. A.: A review of

389 global satellite-derived snow products, Adv. Sp. Res., 50(8), 1007–1029,

390 doi:10.1016/j.asr.2011.12.021, 2012.

391 Geddes, J. A. and Martin, R. V.: Global deposition of total reactive nitrogen oxides from 1996 to

392 2014 constrained with satellite observations of NO2 columns, Atmos. Chem. Phys., 17(16),

393 10071–10091, doi:10.5194/acp-17-10071-2017, 2017.

394 Hall, D. . and Riggs, G. A.: MODIS/Aqua Snow Cover Daily L3 Global 0.05Deg CMG, Version

395 6, , doi:http://dx.doi.org/10.5067/MODIS/MYD10C1.006, 2016a.

396 Hall, D. K. and Riggs, G. A.: Accuracy assessment of the MODIS snow products, Hydrol.

397 Process., 21(12), 1534–1547, doi:10.1002/hyp.6715, 2007.

398   Hall, D. K. and Riggs, G. A.: MODIS/Terra Snow Cover Daily L3 Global 0.05Deg CMG,

399   Version 6, , doi:http://dx.doi.org/10.5067/MODIS/MOD10C1.006, 2016b.

400   Hall, D. K., Fuhrmann, C. M., Perry, L. B., Riggs, G. A., Robinson, D. A. and Foster, J. L.: A

401   Comparison of Satellite-Derived Snow Maps with a Focus on Ephemeral Snow in North

402   Carolina, in 67th Eastern Snow Conference, Hancock MA USA., 2010.

403   Helfrich, S. R., McNamara, D., Ramsay, B. H., Baldwin, T. and Kasheta, T.: Enhancements to,

404   and forthcoming developments in the Interactive Multisensor Snow and Ice Mapping System

405   (IMS), Hydrol. Process., 21(12), 1576–1586, doi:10.1002/hyp.6720, 2007.

406   Herman, J. R. and Celarier, E. A.: Earth surface reflectivity climatology at 340-380 nm from

407   TOMS data, J. Geophys. Res. Atmos., 102(D23), 28003–28011, doi:10.1029/97JD02074, 1997.

408   Kleipool, Q. L., Dobber, M. R., de Haan, J. F. and Levelt, P. F.: Earth surface reflectance

409   climatology from 3 years of OMI data, J. Geophys. Res., 113(D18), D18308,

410   doi:10.1029/2008JD010290, 2008.

411   Koelemeijer, R. B. A., de Haan, J. F. and Stammes, P.: A database of spectral surface reflectivity

412   in the range 335–772 nm derived from 5.5 years of GOME observations, J. Geophys. Res.,

413   108(D2), 4070, doi:10.1029/2002JD002429, 2003.

414   Lamsal, L. N., Janz, S. J., Krotkov, N. A., Pickering, K. E., Spurr, R. J. D., Kowalewski, M. G.,

415   Loughner, C. P., Crawford, J. H., Swartz, W. H. and Herman, J. R.: High-resolution NO2

416   observations from the Airborne Compact Atmospheric Mapper: Retrieval and validation, J.

417   Geophys. Res. Atmos., 122(3), 1953–1970, doi:10.1002/2016JD025483, 2017.

418   Liang, S., Fang, H., Chen, M., Shuey, C. J., Walthall, C., Daughtry, C., Morisette, J., Schaaf, C.

419   and Strahler, A.: Validating MODIS land surface reflectance and albedo products: methods and

420   preliminary results, Remote Sens. Environ., 83(1–2), 149–162, doi:10.1016/S0034-

421   4257(02)00092-5, 2002.

422   Lin, J.-T., Liu, M.-Y., Xin, J.-Y., Boersma, K. F., Spurr, R., Martin, R. and Zhang, Q.: Influence

423   of aerosols and surface reflectance on satellite NO2 retrieval: seasonal and spatial characteristics

424   and implications for NOx emission constraints, Atmos. Chem. Phys., 15(19), 11217–11241,

425   doi:10.5194/acp-15-11217-2015, 2015.

426   Lorente, A., Folkert Boersma, K., Yu, H., Dörner, S., Hilboll, A., Richter, A., Liu, M., Lamsal,

427   L. N., Barkley, M., De Smedt, I., Van Roozendael, M., Wang, Y., Wagner, T., Beirle, S., Lin, J.-

428   T., Krotkov, N., Stammes, P., Wang, P., Eskes, H. J. and Krol, M.: Structural uncertainty in air

429   mass factor calculation for NO2 and HCHO satellite retrievals, Atmos. Meas. Tech., 10(3), 759–

430   782, doi:10.5194/amt-10-759-2017, 2017.

431   Lyapustin, A., Wang, Y. and Frey, R.: An automatic cloud mask algorithm based on time series

432   of MODIS measurements, J. Geophys. Res., 113(D16), D16207, doi:10.1029/2007JD009641,

433   2008.

434   Lyapustin, A., Martonchik, J., Wang, Y., Laszlo, I. and Korkin, S.: Multiangle implementation of

435   atmospheric correction (MAIAC): 1. Radiative transfer basis and look-up tables, J. Geophys.

436   Res., 116(D3), D03210, doi:10.1029/2010JD014985, 2011a.

437   Lyapustin, A., Wang, Y., Laszlo, I., Kahn, R., Korkin, S., Remer, L., Levy, R. and Reid, J. S.:

438   Multiangle implementation of atmospheric correction (MAIAC): 2. Aerosol algorithm, J.

439   Geophys. Res., 116(D3), D03211, doi:10.1029/2010JD014986, 2011b.

440   Lyapustin, A. I., Wang, Y., Laszlo, I., Hilker, T., G.Hall, F., Sellers, P. J., Tucker, C. J. and

441   Korkin, S. V.: Multi-angle implementation of atmospheric correction for MODIS (MAIAC): 3.

442   Atmospheric correction, Remote Sens. Environ., 127, 385–393, doi:10.1016/j.rse.2012.09.002,

443   2012.

444   Martin, R. V, Chance, K., Jacob, D. J., Kurosu, T. P., Spurr, R. J. D., Bucsela, E., Gleason, J. F.,

445   Palmer, P. I., Bey, I. and Fiore, A. M.: An improved retrieval of tropospheric nitrogen dioxide

446   from GOME, J. Geophys. Res. Atmos., 107(D20), 2002.

447   Martin, R. V.: Satellite remote sensing of surface air quality, Atmos. Environ., 42(34), 7823–

448   7843, doi:10.1016/j.atmosenv.2008.07.018, 2008.

449   McLinden, C. A., Fioletov, V., Boersma, K. F., Kharol, S. K., Krotkov, N., Lamsal, L., Makar,

450   P. A., Martin, R. V., Veefkind, J. P. and Yang, K.: Improved satellite retrievals of NO2 and SO2

451   over the Canadian oil sands and comparisons with surface measurements, Atmos. Chem. Phys.,

452   14(7), 3637–3656, doi:10.5194/acp-14-3637-2014, 2014.

453   Menne, M. J., Durre, I., Vose, R. S., Gleason, B. E., Houston, T. G., Menne, M. J., Durre, I.,

454 Vose, R. S., Gleason, B. E. and Houston, T. G.: An Overview of the Global Historical

455 Climatology Network-Daily Database, J. Atmos. Ocean. Technol., 29(7), 897–910,

456 doi:10.1175/JTECH-D-11-00103.1, 2012a.

457 Menne, M. J., Durre, I., Korzeniewski, B., McNeal, S., Thomas, K., Yin, X., Anthony, S., Ray,

458 R., Vose, R. S., Gleason, B. E. and Houston, T. G.: Global Historical Climatology Network -

459 Daily (GHCN-Daily), Version 3.22, , doi:http://doi.org/10.7289/V5D21VHZ, 2012b.

460 National Ice Center: IMS Daily Northern Hemisphere Snow and Ice Analysis at 1 km, 4 km, and

461 24 km Resolutions, Version 1, , doi:http://dx.doi.org/10.7265/N52R3PMC, 2008.

462 Nolin, A., Armstrong, R. and Maslanik, J.: Near real-time SSM/I EASE-grid daily global ice

463 concentration and snow extent, Digit. Media, Natl. Snow Ice Data Center, Boulder, CO, USA,

464 2005.

465 Nowlan, C. R., Martin, R. V., Philip, S., Lamsal, L. N., Krotkov, N. A., Marais, E. A., Wang, S.

466 and Zhang, Q.: Global dry deposition of nitrogen dioxide and sulfur dioxide inferred from space-

467 based measurements, Global Biogeochem. Cycles, 28(10), 1025–1043,

468 doi:10.1002/2014GB004805, 2014.

469 O'Byrne, G., Martin, R. V., van Donkelaar, A., Joiner, J. and Celarier, E. A.: Surface reflectivity

470 from the Ozone Monitoring Instrument using the Moderate Resolution Imaging

471 Spectroradiometer to eliminate clouds: Effects of snow on ultraviolet and visible trace gas

472 retrievals, J. Geophys. Res., 115(D17), D17305, doi:10.1029/2009JD013079, 2010.

473 Palmer, P. I., Jacob, D. J., Chance, K. and Martin, R. V: Air mass factor formulation for

474 spectroscopic measurements from satellites' Application to formaldehyde retrievals from the

475 Global Ozone Monitoring Experiment, J. Geophys. Res., 106(D13), 14,514-539,550, 2001.

476 Richter, A. and Wagner, T.: The Use of UV, Visible and Near IR Solar Back Scattered Radiation

477 to Determine Trace Gases, pp. 67–121, Springer, Berlin, Heidelberg., 2011.

478 Rittger, K., Painter, T. H. and Dozier, J.: Assessment of methods for mapping snow cover from

479 MODIS, Adv. Water Resour., 51, 367–380, doi:10.1016/j.advwatres.2012.03.002, 2013.

480 Spurr, R. J. D.: Simultaneous derivation of intensities and weighting functions in a general

481 pseudo-spherical discrete ordinate radiative transfer treatment, J. Quant. Spectrosc. Radiat.

482   Transf., 75(75), 129–175 [online] Available from: www.elsevier.com/locate/jqsrt (Accessed 20

483   July 2017), 2002.

484   Streets, D. G., Canty, T., Carmichael, G. R., de Foy, B., Dickerson, R. R., Duncan, B. N.,

485   Edwards, D. P., Haynes, J. A., Henze, D. K. and Houyoux, M. R.: Emissions estimation from

486   satellite retrievals: A review of current capability, Atmos. Environ., 77, 1011–1042, 2013.

487   Sun, Q., Wang, Z., Li, Z., Erb, A. and Schaaf, C. B.: Evaluation of the global MODIS 30 arc-

488   second spatially and temporally complete snow-free land surface albedo and reflectance

489   anisotropy dataset, Int. J. Appl. Earth Obs. Geoinf., 58, 36–49, doi:10.1016/j.jag.2017.01.011,

490   2017.

491   Valin, L. C., Russell, A. R. and Cohen, R. C.: Variations of OH radical in an urban plume

492   inferred from NO2 column measurements, Geophys. Res. Lett., 40(9), 1856–1860, 2013.

493   Vasilkov, A., Qin, W., Krotkov, N., Lamsal, L., Spurr, R., Haffner, D., Joiner, J., Yang, E.-S.

494   and Marchenko, S.: Accounting for the effects of surface BRDF on satellite cloud and trace-gas

495   retrievals: a new approach based on geometry-dependent Lambertian equivalent

496   reflectivity applied to OMI algorithms, Atmos. Meas. Tech., 10(1), 333–349, doi:10.5194/amt-

497   10-333-2017, 2017.

498   Warren, S. G. and Wiscombe, W. J.: A Model for the Spectral Albedo of Snow. II: Snow

499   Containing Atmospheric Aerosols, J. Atmos. Sci., 37(12), 2734–2745, doi:10.1175/1520-

500   0469(1980)037<2734:AMFTSA>2.0.CO;2, 1980.

501   Yang, J., Jiang, L., Ménard, C. B., Luojus, K., Lemmetyinen, J. and Pulliainen, J.: Evaluation of

502   snow products over the Tibetan Plateau, Hydrol. Process., 29(15), 3247–3260,

503   doi:10.1002/hyp.10427, 2015.

504   Zoogman, P., Liu, X., Suleiman, R. M., Pennington, W. F., Flittner, D. E., Al-Saadi, J. A.,

505   Hilton, B. B., Nicks, D. K., Newchurch, M. J., Carr, J. L., Janz, S. J., Andraschko, M. R., Arola,

506   A., Baker, B. D., Canova, B. P., Chan Miller, C., Cohen, R. C., Davis, J. E., Dussault, M. E.,

507   Edwards, D. P., Fishman, J., Ghulam, A., González Abad, G., Grutter, M., Herman, J. R., Houck,

508   J., Jacob, D. J., Joiner, J., Kerridge, B. J., Kim, J., Krotkov, N. A., Lamsal, L., Li, C., Lindfors,

509   A., Martin, R. V., McElroy, C. T., McLinden, C., Natraj, V., Neil, D. O., Nowlan, C. R.,

510   O'Sullivan, E. J., Palmer, P. I., Pierce, R. B., Pippin, M. R., Saiz-Lopez, A., Spurr, R. J. D.,

511   Szykman, J. J., Torres, O., Veefkind, J. P., Veihelmann, B., Wang, H., Wang, J. and Chance, K.:

512   Tropospheric emissions: Monitoring of pollution (TEMPO), J. Quant. Spectrosc. Radiat. Transf.,

513   186, 17–39, doi:10.1016/j.jqsrt.2016.05.008, 2017.

514

515

516
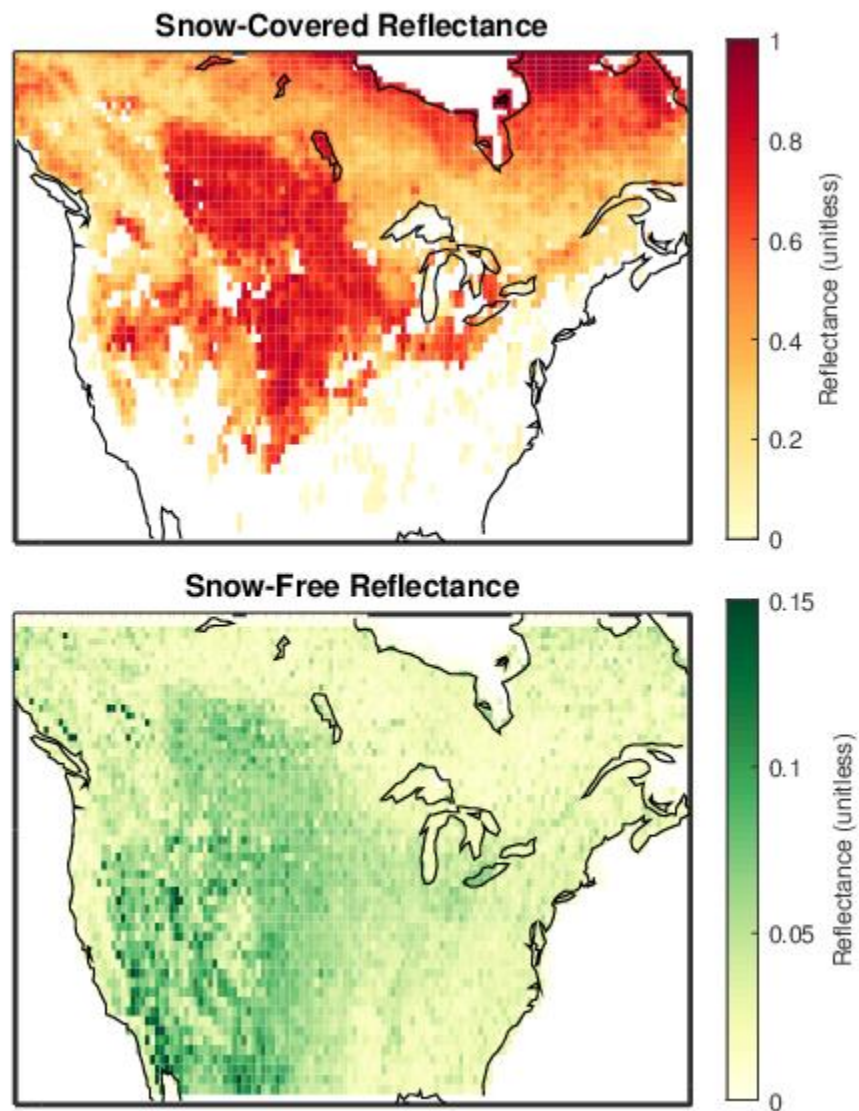
Figure 1: Surface reflectivity at UV-visible wavelengths for snow-covered and snow-free

conditions for January 2013. White space in top panel indicates no snow reflectance information

is available.

520

521
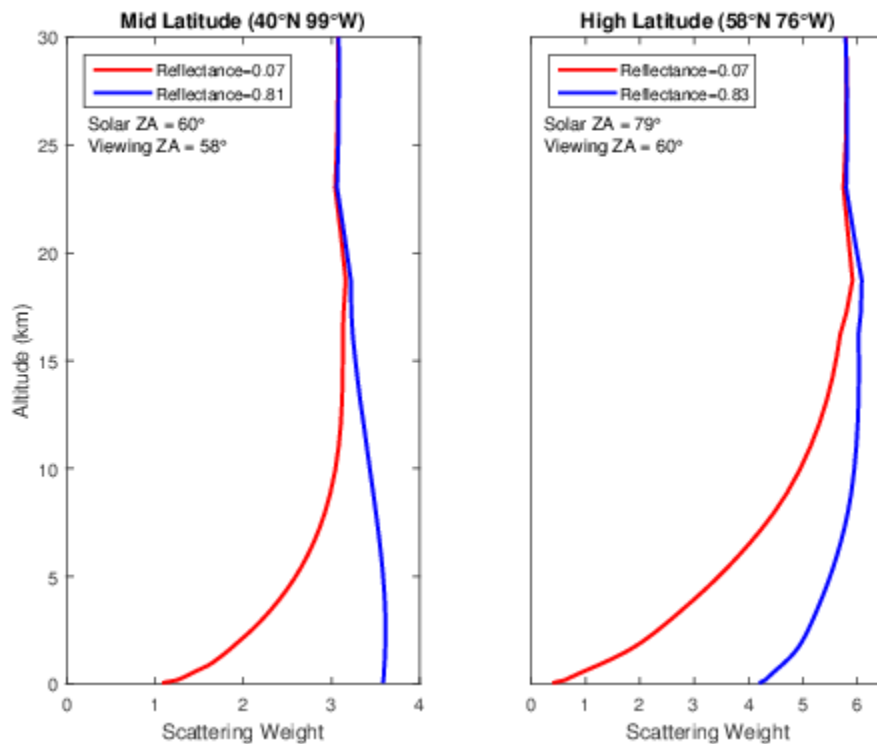
Figure 2: Observation sensitivity to NO_2. Scattering weight profiles calculated for cloud-free

OMI NO_2 retrievals, with and without surface snow cover, for January 2013 at (Left) 42° N, 99°

W with a solar zenith angle (ZA) of 60° and (Right) 58° N, 76° W with a solar zenith angle of

79°.

526
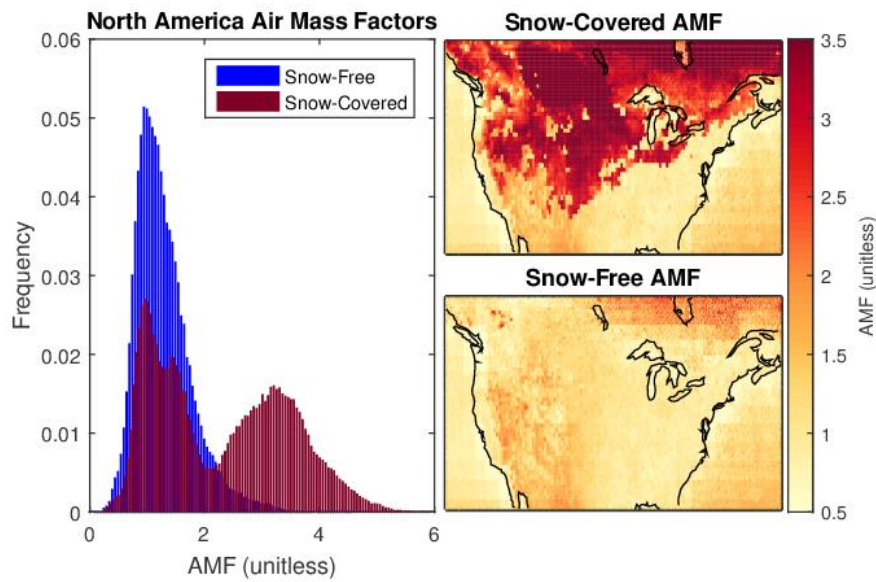
527

528   Figure 3: (Left) Distribution of Air Mass Factors (AMFs) calculated for OMI NO$_2$ retrievals over

529   North America for observation geometry of January 2013, with and without surface snow cover.

530   (Right) Maps of AMF for snow-covered and snow-free conditions.

531
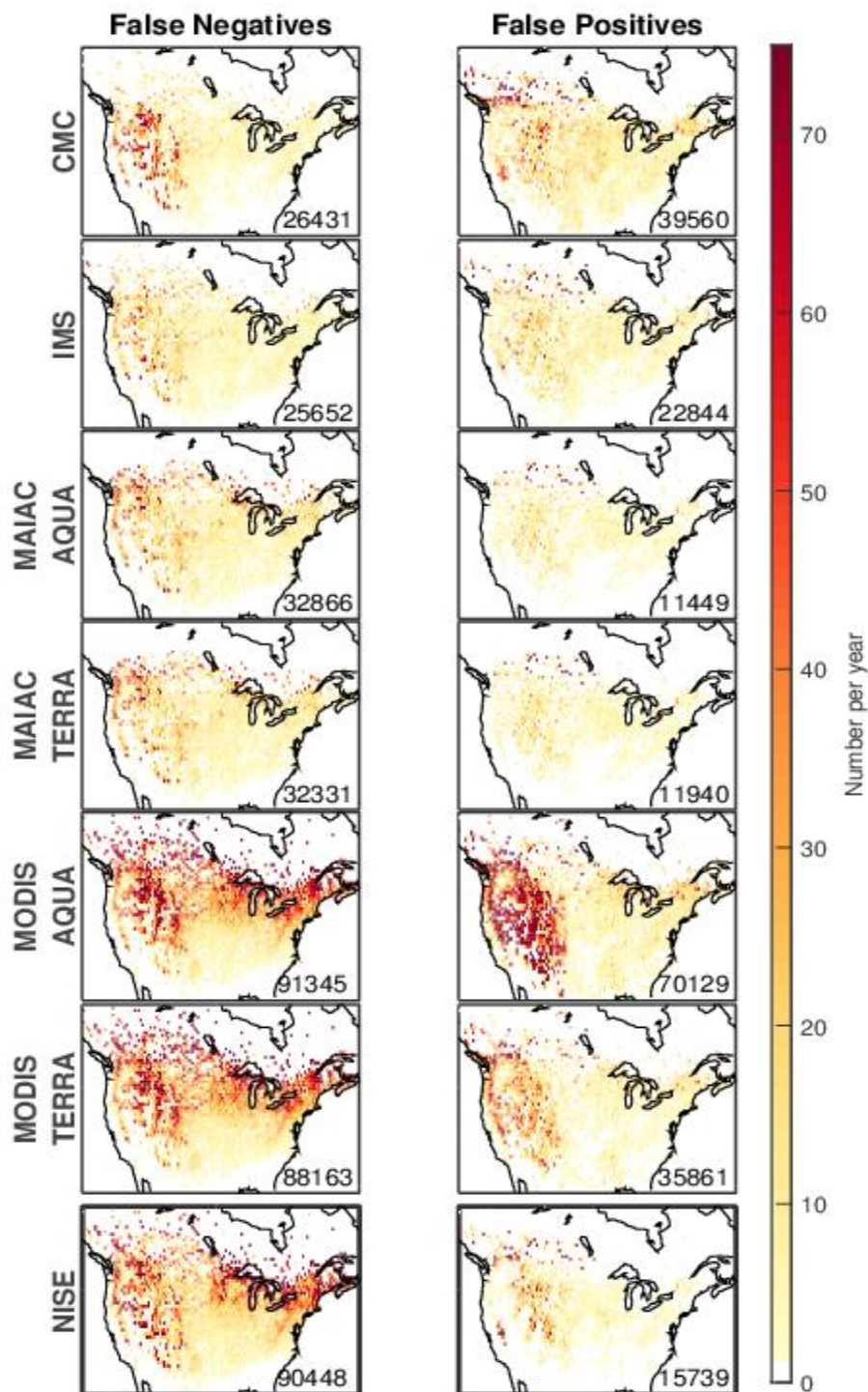
Figure 4: Number of false positive (FP) and false negative (FN) snow attributions by the snow

data sets in 2015. All data sets are evaluated at 4 km resolution. Total number of false snow

attributions inset. White space indicates no ground stations present.

535
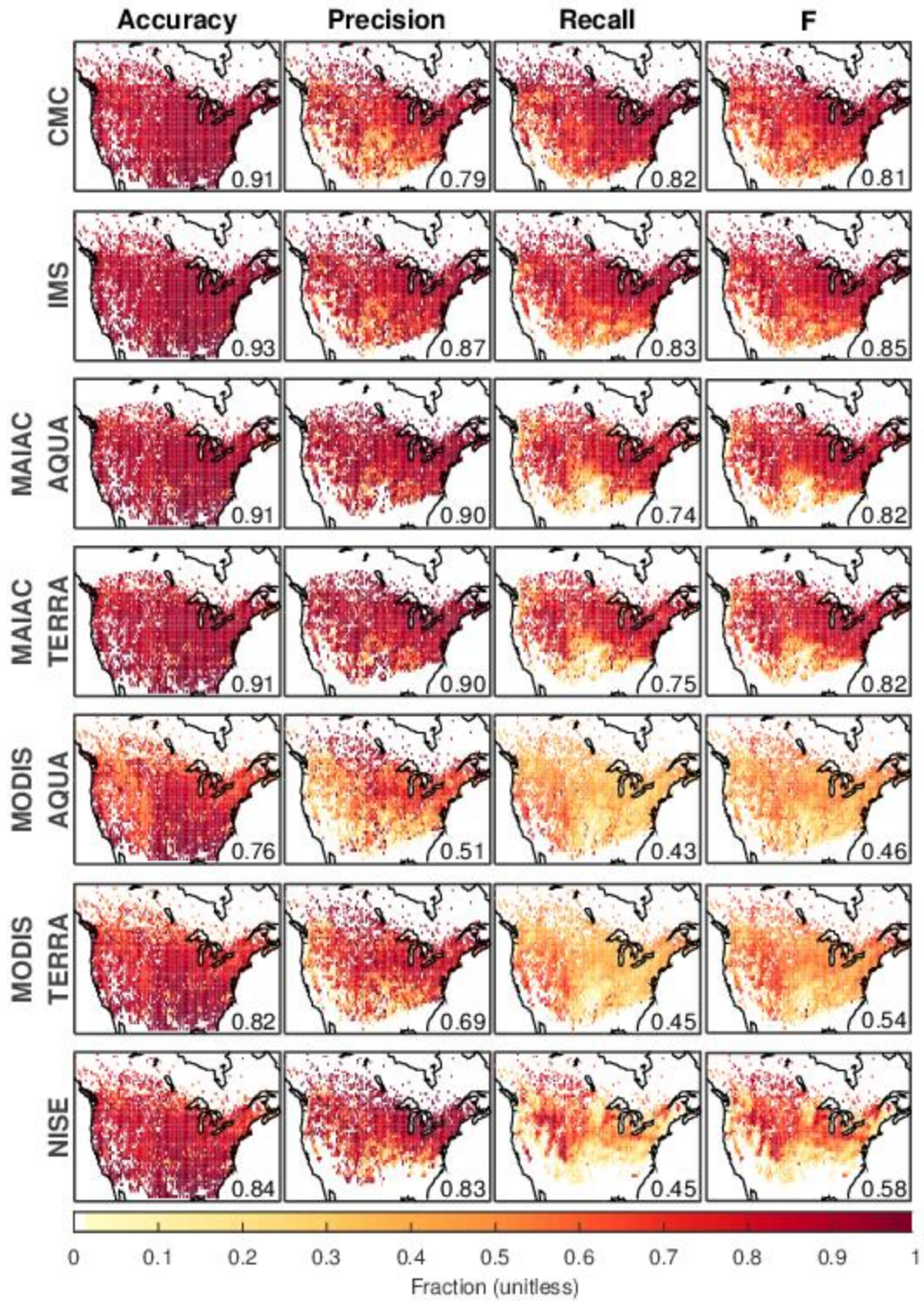
Figure 5: Statistical metrics to evaluate snow cover products. All data sets are gridded at 4 km
resolution. White space indicates no ground stations present.
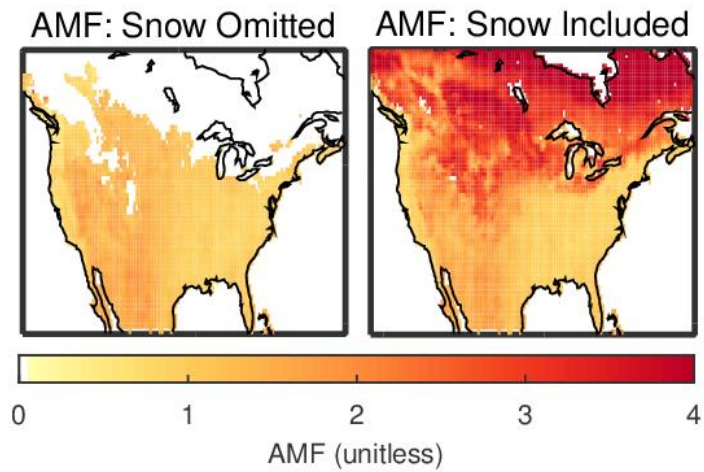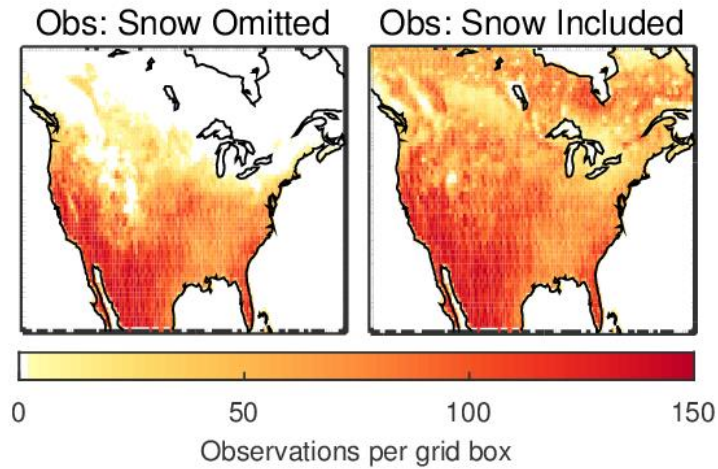
Figure 6: OMI observation frequency (top) and average AMFs (bottom) over North America in January using IMS to identify surface snow conditions. White space indicates a lack of observations.

543

	Accuracy	Precision	Recall	F
CMC	0.91	0.79	**0.83**	0.81
IMS	**0.93**	0.87	**0.83**	**0.85**
MAIAC AQUA	0.91	**0.90**	0.74	0.82
MAIAC TERRA	0.91	**0.90**	0.75	0.82
MODIS AQUA	0.76	0.51	0.43	0.46
MODIS TERRA	0.82	0.69	0.45	0.54
NISE	0.84	0.83	0.45	0.58

544 Table 1: Evaluation of daily snow extent data set performance for 2015. GHCN-D surface

545 observations are used as "truth". All products are regridded to a common 4 km resolution. The

546 highest value for each metric is shown in bold.

547 **Appendix**

Months	Data Set	Accuracy	Precision	Recall	F
	CMC	0.84	0.84	0.89	0.86
	IMS	**0.88**	0.90	**0.88**	**0.89**
	MAIAC AQUA	0.84	**0.93**	0.80	0.86
DJF	MAIAC TERRA	0.84	0.92	0.80	0.86
	MODIS AQUA	0.58	0.84	0.34	0.48
	MODIS TERRA	0.60	0.88	0.37	0.52
	NISE	0.63	0.90	0.41	0.57
	CMC	0.90	0.63	0.57	0.59
	IMS	**0.93**	0.74	**0.67**	0.70
	MAIAC AQUA	**0.93**	**0.81**	0.62	**0.71**
MAM	MAIAC TERRA	**0.93**	**0.81**	0.63	**0.71**
	MODIS AQUA	0.86	0.43	0.39	0.41
	MODIS TERRA	0.89	0.62	0.40	0.49
	NISE	0.90	0.71	0.34	0.46
	CMC	0.91	0.73	**0.81**	0.76
	IMS	**0.92**	0.82	0.74	**0.78**
	MAIAC AQUA	0.91	**0.86**	0.60	0.71
SON	MAIAC TERRA	0.90	0.85	0.61	0.71
	MODIS AQUA	0.82	0.51	0.36	0.42
	MODIS TERRA	0.86	0.71	0.39	0.51
	NISE	0.85	0.85	0.25	0.39

548 Table A1: Evaluation of daily snow extent data set performance by season for 2015. GHCN-D

549 surface observations are used as "truth". All products are regridded to a common 4 km

550 resolution. The highest value for each metric/season is shown in bold.

551

	Resolution	Accuracy	Precision	Recall	F
CMC	25 km	0.92	0.81	0.81	0.81
IMS	4 km	**0.93**	0.87	**0.83**	**0.85**
MAIAC AQUA	1 km	0.91	**0.91**	0.71	0.80
MAIAC TERRA	1 km	0.91	0.90	0.71	0.80
MODIS AQUA	0.05°	0.77	0.50	0.30	0.37
MODIS TERRA	0.05°	0.81	0.65	0.32	0.43
NISE	25 km	0.85	0.87	0.37	0.51

553 Table A2: Evaluation of daily snow extent data set performance for 2015. GHCN-D surface

554 observations are used as "truth". The highest value for each metric is shown in bold.

555

	Accuracy	Precision	Recall	F
CMC	0.92	0.81	0.81	0.81
IMS	**0.93**	0.84	**0.85**	**0.84**
MAIAC AQUA	0.87	0.69	0.73	0.71
MAIAC TERRA	0.88	0.68	0.73	0.71
MODIS AQUA	0.78	0.50	0.41	0.45
MODIS TERRA	0.83	0.68	0.43	0.53
NISE	0.85	**0.87**	0.37	0.52

556 Table A3: Evaluation of daily snow extent data set performance for 2015. GHCN-D surface

557 observations are used as "truth". All products are regridded to a common 25 km resolution. The

558 highest value for each metric is shown in bold.